Egypt. J. Chem. Vol. 64, No. 9 pp. 4889 - 4899 (2021)

Egyptian Journal of Chemistry

http://ejchem.journals.ekb.eg/

Fabrication and Characterization of Hydrophobic PVDF-based Hollow Fiber Membranes for Vacuum Membrane Distillation of Seawater and Desalination Brine

Mohamed H. Sorour, Heba A. Hani*, Hayam F. Shaalan, Mahmoud El-Toukhy

Chemical Engineering and Pilot Plant Department, National Research Centre, El-Buhouth Street, Dokki, Giza, Egypt; P.O. Box 12622

Abstract

Fabrication of hydrophobic polyvinylidene fluoride (PVDF) hollow fiber membranes was studied using Lithium chloride (LiCl) and polyethylene glycol (PEG 35000) as non-solvent additives by dry-wet phase inversion process. Scanning Electron Microscopy revealed that LiCl addition made the finger-like voids become smaller and provided a sponge-like structure, in addition to increasing the membrane surface roughness to 42 nm, porosity to 83% and mean pore size to 5.75 nm with narrower pore size distribution. It also decreased Young's modulus to 63 MPa while, no significant improvement was observed in water contact angle (115.5º). During vacuum membrane distillation (VMD) of water, Mediterranean Sea water, Red Sea water and Red Sea brine, the PVDF membranes spun with LiCl achieved higher water permeation flux with values of 48, 32, 25 and 19 L/m^{2}h, respectively. The flux-salinity relationship was represented by empirical correlations. The two membranes exhibited high salt rejection values (99.4%-99.8%) for the investigated saline solutions. These results suggest numerous interventions for membrane distillation within integrated desalination/salt recovery schemes or as a stand-alone facility with the combination of complementary appropriate thermal crystallization units. Two VMD/solar pond scenarios were investigated for dual production of water and salts.

Keywords: Hydrophobic hollow fiber membrane, PVDF, vacuum membrane distillation, seawater and brine

1. Introduction

Membrane distillation (MD) is an emerging energy-intensive low-pressure membrane separation technology enabling combined production of freshwater and concentrated brine. The thermal gradient between feed and permeate compartments drives vapor from the former to the latter compartment [1–3]. Four main configurations exist for different MD applications comprising direct contact (DCMD), vacuum (VMD), sweeping gas (SGMD) and air gap (AGMD) [1,3]. Comparing the two most common applied configurations DCMD and VMD reveals that the heat loss from the saline water due to thermal conduction and the temperature polarization on the permeate side are lower in VMD, in addition to higher water vapor flux that could be achieved when applying a reasonably high vacuum [4]. Hollow fiber membranes have recently received much attention in MD due to their high surface area to volume ratio, low footprint and ease of handling during fabrication [2,5,6]. Three direct features characterize MD as compared to other membrane separation processes. The first is related to the hydrophobic nature of the membrane which is of current interest among concerning membrane community and it is a necessary condition for the successful performance of MD. Non wetting hydrophobic membranes are usually used in the membrane distillation process. Many Polymers have been used to fabricate these types of membranes including polyvinylidene fluoride (PVDF), polypropylene (PP), and polytetra- fluoroethylene

*Corresponding author e-mail: hi_heba2@yahoo.com.; (dr.hebahani@gmail.com).
Receive Date: 20 March 2021, Revise Date: 09 May 2021, Accept Date: 09 May 2021
DOI: 10.21608/EJCHEM.2021.68699.3500

(PTFE). Generally, the excellent performance in MD could be achieved by using membrane with good thermal and mechanical stabilities, low thermal conductivity, low wetting resistance and low resistance to mass transfer [3,7,8]. The second important feature is the possibility of using solar energy or an appropriate waste heat source for powering the MD units. Thus, remote coastal and desert communities in arid areas could be served by this type of technology [9–11]. Also, electric power plants working with seawater cooling can be coupled with MD units for additional water production. The third feature is related to the great versatility of this process which permits seawater/brine concentration to the level of overall or differential source crystallization in addition to integrating MD with nano filtration (NF) or reverse osmosis (RO) for water desalination [12–14]. The ability to process and concentrate brines from membrane and thermal desalination plants guarantees additional water production and highly concentrated brines suitable for salt recovery. In this sense, MD technology enables higher recovery desalination and salt crystallization to be undertaken simultaneously [15–17]. The most important limitations of using MD are excessive energy consumption, aggressive fouling of membrane surface and immaturity of the technology. Several additives were used for modification of membranes' properties and accordingly, enhance the MD performance [18,19].

Given the limited research on MD application to Red Sea water, this work presents a detailed study using VMD system to produce fresh water from Mediterranean Sea water and Red Sea water, as well as Red Sea brine using developed hydrophobic PVDF HF membranes prepared using different additives. Attempts were made to investigate the effect of additives on membrane characteristics, pure water permeability and salt rejection and also to correlate the flux-salinity relationship. Moreover, two scenarios were proposed and investigated for dual production of water and salts through mass balance which is based on the results of this study, in addition to other technical parameters.

2. Experimental

2.1. Materials

Polyvinylidene fluoride (PVDF) was supplied from Alfa Aeser, Germany and used as the base polymer. Dimethylacetamide (DMAc) and dimethylformamide (DMF) were supplied from Carl-Roth and Merck, respectively and used as solvents without further purifications. Poly ethylene glycol (PEG) soluble polymer with molecular weight 35000 was supplied from Merck and used as non-solvent additive. Lithium chloride (LiCl) was supplied from Alpha Chemika and used as small molecular pore former inorganic salt non-solvent additive. Distilled water (DW) water was used as the bore fluid and in coagulation and washing baths.

Three saline solutions were tested for VMD comprising Mediterranean Sea water (Marsa matrooh, Egypt), Red Sea water (Safaga, Egypt) and finally Red Sea brine (thermally concentrated Red Sea water). The pH values of these solutions range from 7.6-7.85. Table 1 shows the composition and main characteristics of the investigated saline solutions.

Table 1: Composition and main characteristics of the selected saline solutions

Parameter *	Seawater		Red Sea brine
	Mediterranean	Red Sea	
Ca^{2+}	400	488	756
Mg^{2+}	1460	1660	2573
Na^{+}	11000	13538	20984
Cl^{-}	20000	24350	37743
SO_4^{2-}	2700	3352	5196
K^{+}	500	551	854
CO_3^{2-}	20	28.8	44.6
HCO^{3-}	90	102.5	158.9
Alkalinity	110	132	204.6
TDS	36320	44200	68514
Conductivity, µs	54800	65389	97976

* All concentrations are in mg/L

2.2. Methods

2.2.1. PVDF HF membrane fabrication

Dope preparation

The PVDF powder was dried at 100ºC for 24 h to remove its moisture content before it was used for dope preparation. Certain amount of PVDF (20 wt%) powder was dissolved into the mixture of (10:1) DMF/DMAc solvent and non-solvent additives (3 wt% PEG and 2 wt% LiCl), then the polymer dope mixture was subjected to continuous stirring for about 4-5 days at 70ºC and 1-3 bar under nitrogen until a homogeneous solution was formed. Two samples were prepared, the first sample (PV) was

prepared using only PEG as the non-solvent additive while, the second sample (PVL) was prepared similarly but with the addition of LiCl. The solutions were degassed under vacuum condition and left stagnant until spinning.

Spinning of PVDF HF membranes

PVDF HF membranes were fabricated through a dry-wet phase inversion spinning process as described previously by the authors [20] on a semi-pilot scale spinning facility. Briefly, the polymeric dope was prepared in a stirred tank jacketed vessel then it was pumped using a metering pump and extruded through an annular spinning nozzle supported on a heated spin block. Bore fluid (lumen side) was supplied from a pressurized vessel (0.5-2 bar) and fed to the spinneret passing in the center of the annulus to preserve the hollow structure within the fibers. The as-spun fibers discharged from the spin block were introduced into a water filled coagulation bath to solidify then, collected and wrapped multiple times and fed to two consecutive washing baths where they were rolled again and finally wound on a take-up reel winder. Prepared fibers have been soaked thoroughly in distilled water for removal of excess solvent and left to dry ambiently. Spinning conditions are shown in Table 2.

Module preparation

A bundle of ten dry PVDF fibers have been potted in a glass module of 2.5 cm inside diameter and 25 cm active fiber length using epoxy resin to pot both ends of the fiber and then, the fibers were cut open from both sides to accommodate lumen side-feed configuration in an (in-out) mode.

Table 2: Spinning conditions for PVDF HF membranes

Investigated parameter	Value
Dope flow rate, mL/min	4.5
Bore fluid flow rate, mL/min	2.6
Air gap, cm	25
Spinning temperature, ^{O}C	65
Coagulation bath temperature, ^{O}C	20
Washing bath temperature, ^{O}C	20
Take–up speed, m/min	9.5-10.5
Spinneret dimensions, µm	D_i/D_{out}: 500/1200

2.2.2. PVDF HF membrane characterization

SEM

The morphology of both PVDF HF membranes was studied through SEM imaging using scanning microscopes JEOL-JXA-840 A and JEOL SEM 6000 Neoscope desktop. HF membrane samples were cut using a sharp razor and then they were fixed on the sample stage using carbon double-face tape. Morphological structure and HF membrane inside and outside diameter, as well as, wall thickness were evaluated. The SEM microscope is coupled with an electron dispersive spectrum (EDS), which was used for elemental analysis of the prepared PVDF HF membranes.

AFM

PVDF HF membrane surface roughness were analyzed using 1.5 micron resolution TT-AFM workshop, equipped with a video optical microscope with up to 400X zoom. A one cm long fiber sample was fixed using a double face tape on the magnetic plate of the AFM apparatus. Vibrating scan mode was used for testing a scan area of 5 µm × 5 µm. Roughness parameters were calculated using "Gwidyyon" software.

Hydrophobicity

Moreover, the hydrophobicity of the fibers was evaluated by measuring their contact angles. The water contact angle (WCA) of the HF membrane was measured on an Attention Theta optical contact angle instrument (KSV Instruments Ltd) through a digital video image of the water drop of 5 µL volume on the dried surface of the hollow fiber at 25°C. All the samples were tested at five different positions and the final results presented are an average of the measured values.

Average porosity

The porosity of the fibers was measured using the gravimetric method according to the procedure described previously [21] by measuring the weight of the liquid entrapped within the membrane pores. The overall porosity was calculated according to the following formula:

$$\varepsilon\,(\%) = \frac{\frac{(w_1 - w_2)}{D_k}}{\frac{(w_1 - w_2)}{D_k} + \frac{w_2}{D_{pol}}} * 100 \qquad (1)$$

where w_1 is the weight of the wet membrane, w_2 the weight of the dry membrane, D_k the density of

kerosene (0.82 g/cm^3), D_{pol} is the density of PVDF (1.78 g/cm^3). For each fiber type, five measurements were carried out and average values are presented.

Mean pore size and pore size distribution

Mean pore size and pore size distribution for the prepared PVDF HF membranes were determined using pore size distribution analyzer Belsorp Max apparatus (MicrotracBel. Corp.). Adsorptive nitrogen was used at 77 K. Vacuum degree before measurement was 6.95E^{-4} Pa and standard vapor pressure was 108 kPa.

Average pore size was also determined through hydraulic permeability using the Hagen- Poiseuille equation which gives the relation- ship between the pure water flux (using distilled water at 25^{o}C) and the applied pressure across the membrane (0.1 MPa) for certain time, as well as, the average porosity of the membrane, according to the following equation [20,22].

$$J_s = \frac{r_p^2 * \Delta P}{8 * \mu * \frac{\Delta x}{\varepsilon}} \quad (2)$$

where J_s is the water flux based on membrane area (m/s), r_p is the average effective pore radius (m), ΔP is the transmembrane pressure (Pa), μ is solution viscosity (Pa.s), Δx is the effective membrane thickness (m) and ε is the membrane porosity (volume %).

Mechanical properties

Mechanical properties of PVDF HF membranes were studied using a benchtop tensile testing machine (Tinius Olsen H5kS) equipped with a 5N load cell. Testing was undertaken at 50 mm/min speed and a gauge length of 100 mm. Tensile stress, elongation at break and fiber's Young's modulus were measured.

2.2.3. Vacuum membrane distillation experiments

VMD experimental set-up used for testing the permeation performance of the prepared PVDF HF membranes is shown in Figure. 1. VMD experiments were performed using distilled water, Mediterranean Sea water, Red Sea water and Red Sea brine. A membrane module was mounted vertically in the system to reduce the effect of free convection and eliminate air bubbles. The system is equipped with flow meters, pressure sensors and thermocouples. In this system, the saline solution is fed to a jacketed feed tank which is heated to 70^{o}C using a temperature-controlled circulating water bath. The hot solution is fed to the membrane module with a flow rate of 3.3 cm^3/s. The feed passes through the lumen side of the module and the reject was returned to the feed tank where the vacuum is applied on the shell side. The VMD system was operated within brine concentration regime to avoid intra-fiber occlusion. The vapors were transported through the membrane and then condensed in a stainless steel tubular condenser which is connected to a vacuum pump, with vacuum degree less than 0.1 mbar, and cooled to a temperature of about 1-2^{o}C using a chiller. The condensed permeate was collected in a separate tank where a sample was taken every 30 min, weighed, by an electronic balance, and its electrical conductivity was measured, using a conductivity meter, in order to check fiber salt rejection. Average flux values were represented for 5-6 samples. The volume of the distillate collected after specific time intervals was measured and the VMD permeate flux (J: L/m^2.h) was calculated according to the following relation:

$$J = Q/A \quad (3)$$

where Q represents vapor permeate flow (L/h), A is the effective membrane area calculated based on membrane inner diameter, length of each fiber and the total number of fibers (m^2). Moreover, salt rejection (R%) values were calculated using the following equation:

$$R\ (\%) = (1-(C_p/C_f)) * 100 \quad (4)$$

where C_p and C_f are the concentrations of permeate and feed streams, respectively.

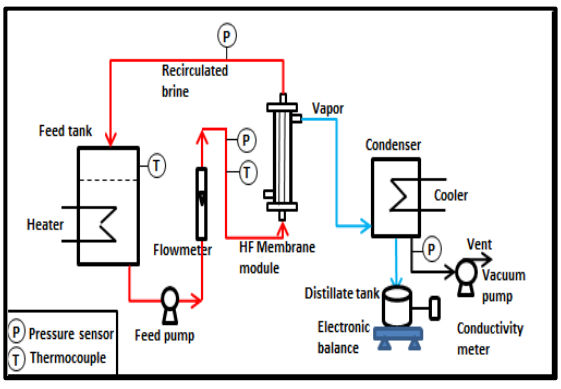

Fig.1. Schematic of vacuum membrane distillation experimental set-up

3. Results and Discussion

3.1. PVDF HF membranes morphology

3.1.1. SEM

The SEM images of the prepared PVDF HF membrane samples has been determined and presented in Figure 2 illustrating i) fibers cross-section, ii) wall thickness and iii) surface. The images in Figure 2a reveal asymmetric morphology consisting of finger-like macrovoids near the inner and outer surfaces of the PV HF fibers and sponge-like structure in the middle. The sponge-like structure is related to the relatively high polymer concentration (20%) used of viscosity (4100 cp), which delays the solvent-non-solvent exchange for coagulation and thus slows down polymer solidification [23]. The voids formed were attributed to PEG presence where, non-solvent additives such as PEG in dopes may cause large cavities in the membrane [24], which compensates the tendency for sponge-like structure due to PVDF used. Figure 2b presents the SEM images for the PVL HF membrane sample. Lithium chloride addition makes the finger-like macrovoids beneath the outer and inner layers of the fiber become smaller and longer and provided more sponge like structure. LiCl is thought to benefit the solid-liquid demixing process and suppress macrovoid formation, which may be related to the increase in the spinning dope viscosity (5800 cp) caused by the interaction of LiCl with solvent, as well as, with electron donor group of PVDF to delay the dope precipitation [25–28]**.** It should be noted that the finger/sponge like structure resulted from the addition of LiCl comprise a trade-off choice between permeability and wetting resistance [29]. Average values of inside and outside diameters of PV and PVL HF membranes were 630, 561 µm and 875, 789 µm, respectively**.**

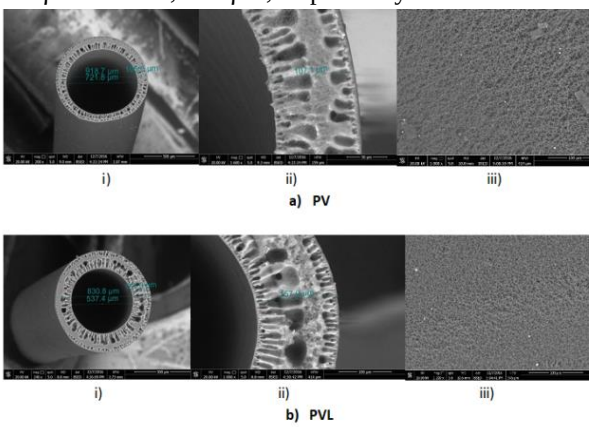

Fig.2. SEM images of PVDF HF membranes

The EDS results show that the prepared PVDF HF membranes are mainly formed from the fluoride and carbon elements with comparable values for PV and PVL membranes, as shown in Figure 3. The atomic % of carbon, nitrogen, fluoride and oxygen were comparable for both samples representing 54.2, 0.2, 42 and 3.4%, respectively.

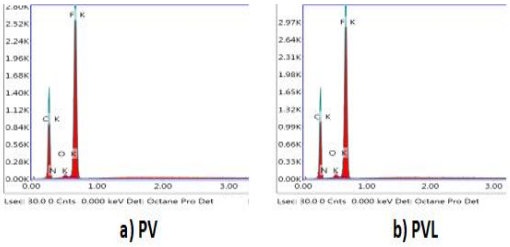

Fig.3. EDS of the prepared PVDF HF membranes

3.1.2. AFM

AFM images of the prepared PVDF HF membranes have been obtained and presented in Figure 4. The surface roughness values (Ra and Rms), as depicted in Table 3**,** are higher in the case of PVL which is attributed to the presence of the pore former, LiCl that alters the membrane's surface and increases surface roughness accordingly [27].

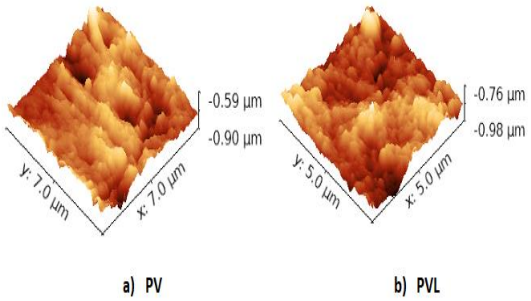

Fig.4. AFM images of the prepared PVDF HF membranes

3.1.3. Membrane hydrophobicity

The surface hydrophobicity of the PV and PVL HF membranes was evaluated by water contact angle measurements, and the results are shown in Figure 5. Comparable water contact angle values, with minor increase for the PVL membrane, (114^{o} and 115.5^{o}) were obtained for both PVDF membranes, indicating high hydrophobicity of the fabricated membranes. These values are considered relatively higher than those reported by Tang et al. [28]**.**

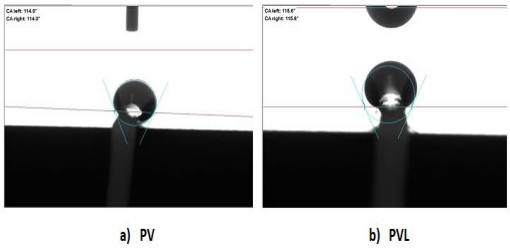

Fig.5. Water contact angle images of the prepared PVDF HF membranes

3.2. Membrane porosity

The porosities of the prepared PVDF HF membranes (PV and PVL), determined by the gravimetric method, are shown in Table 3. It is noticed that LiCl addition has increased the porosity of the fibers from 78% to 83%. These values generally agree with the published range (69%-92%) for PVDF hollow fibers [21,28,30,31].

3.3. Membrane pore size and pore size distribution

The pore size of the prepared PVDF HF membranes was determined by using pore size distribution analyzer Belsorp Max apparatus (MicrotracBel. Corp.) and Hagen- Poiseuille equation (equation 2). The mean pore size values of PV and PVL determined by Belsorp analyzer were 4.646 and 5.639 nm, respectively while those calculated by equation 2 were 4.456 and 5.753 nm, respectively. The values are comparable and agree with Mansouri et al. who used 2 and 4% LiCl with PVDF [29]. It was previously proved that the smaller pore sizes are more capable to capillary condensation based on the Kelvin equation [32].

The pore size distribution of the membranes was determined by using the Belsorp Max apparatus and shown in Figure 6**.** It is obvious that the PVDF HF membrane spun with 2% LiCl revealed higher pore size and narrower pore size distribution which agrees with published work [24,27].

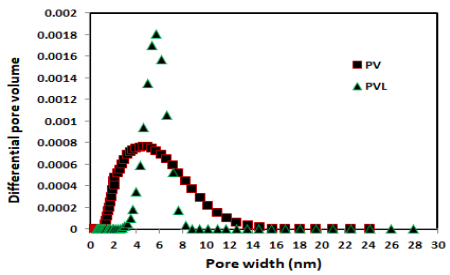

Fig.6. Pore size distribution for the prepared PVDF HF membranes

3.4. Membrane mechanical properties

Mechanical properties of PVDF membranes were and the stress-strain curves were measured and are shown in Figure 7. It is observed that PV has higher mechanical properties than PVL. This has been explained previously [33,34] where the addition of LiCl decreased mechanical properties but enhanced the membrane's permeation rate. Average and standard deviation (SD) values of break force (N), break stress (tensile strength: MPa), elongation at break (break strain: %) and Young's modulus (MPa) for the prepared membranes are presented in Table 3. The results agree with the increase in porosity discussed in section 3.2.

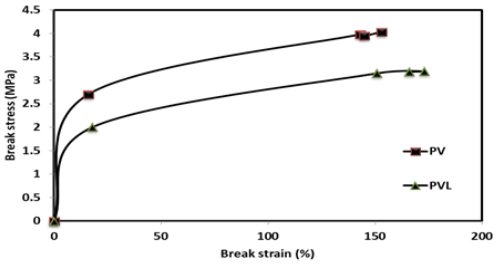

Fig.7. Stress strain curve for the prepared PVDF HF membranes

Table 3: Characteristics of the prepared PVDF HF membranes (PV and PVL)

Property	PV	PVL
a. Fibers morphology		
ID (µm)	630	561
OD (µm)	875	789
Thickness (µm)	123	149
b. Mechanical properties		
Break force (N) Average/SD	0.97/0.0224	1/0.00654
Break stress (MPa) Average/SD	4.03/0.0928	3.18/0.0208
Break strain (%) Average/SD	153/9.94	166/10.3
Young's modulus (MPa) Average/SD	74.8/17.6	63.3/14.3
c. AFM results		
Ra (nm)	32.7	42
Rms (nm)	41.2	53
Porosity (%)	78.4	83.4
Average pore size (nm)	4.646	5.7531
d. Hydrophobicity		
Water contact angle (°)	114	115.5

3.5. Water permeability of PVDF HF membranes applied in VMD experiments

3.5.1. Test on distilled water

The pure water flux experiments were conducted for PV and PVL at 70°C under VMD mode and the flux values were 37.6 and 48 L/m^{2}h for PV and PVL, respectively as presented in Table 4. This may be attributed to the higher porosity obtained after the addition of LiCl, which agrees with results mentioned in the previous sections, where the addition of pore former additive in the polymer dopes generally results in the enhancement of liquid-liquid demixing which enhances the membrane porosity and, consequently, the VMD flux [4,26,28,29,35]. It is worth mentioning that these values are higher than those previously published under comparable VMD conditions for PVDF HF membranes [4,30,31,36,37], but lower than those published by Drioli et al. who used PVP and maleic acid as additives [21].

3.5.2. Test on saline solutions

Three saline solutions were tested under VMD mode and it is noticed that salinity is reduced by 99.4-99.8% for all the studied saline solutions.

The VMD/permeate flux of different saline solutions using PVDF HF membranes have been measured as depicted in Figure 8. It is clear that the flux values obtained using PV HF membrane decreased from 23 L/m^{2}h in the case of Mediterranean Sea water to 18 L/m^{2}h for Red Sea water and finally to 14 L/m^{2}h using Red Sea brine. It is worth mentioning that PVL HF membrane prepared using LiCl achieved higher flux values of 32, 25 and 19 L/m^{2}h for the three tested saline solutions. This may be attributed to the role of LiCl as mentioned earlier. Moreover, two empirical correlations have been formulated representing the relation between flux and the studied feed salinities for the two prepared membranes, as represented in Figure 8 and in equation no. (5) for PV and equation no. (6) for PVL HF membranes.

$$\text{VMD flux} = -0.44 * \text{Feed salinity} + 47.3 \quad (5)$$

$$\text{VMD flux} = -0.35 * \text{Feed salinity} + 36.1 \quad (6)$$

These flux values are higher than those previously published by Huyan et al., where the VMD flux using 3.5% NaCl was 28 L/m^{2}h at 70°C which decreased to 20L/m^{2}h using seawater (38.9 g/L) at 70°C [38]. Tang et al. studied the PVDF HF membrane performance, prepared using 2.6% LiCl, under VMD mode and revealed 23 L/m^{2}h using 9% NaCl [28]. Synthetic seawater was studied by Simone et al. and revealed flux value ranging from 12-14.5 L/m^{2}h on varying the feed flow rate from 27 L/h to 32 L/h at 50°C [30,31] . Further, a pilot-scale PVDF HF membrane with a total membrane area of 5.4 m^2 was tested on seawater for VMD with solar heating system and attained 8 L/m^{2}h [39]. Also, the effect of salinity on the final flux at 75°C and 45, 35 and 25 g/L was studied recording 11, 10 and 9 L/m^{2}h [39]. The obtained results reflect a rather energy conservation mode due to complete or partial recirculation, simulating multistage processing at temperature about 70°C which is more practical under normal field conditions[36]. Table 4 represents a comparison between the main characteristics and flux of different PVDF HF membranes studied in literature and in this study.

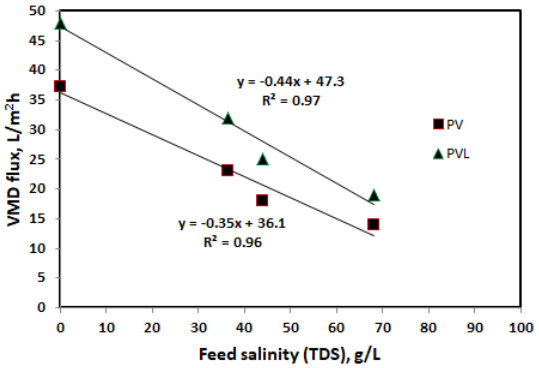

Fig.8. VMD flux of PVDF HF membranes at different feed salinities

3.6. Implications on process design of VMD based system

The results of this work strongly support the technical feasibility of desalination and concentration of Mediterranean Sea water and Red Sea water using multi-stage VMD. Where, previous studies incorporated solar-assisted VMD [10,40,41], solar-assisted multistage VMD [42,43], multistage VMD [44–46] and multistage pilot-scale VMD [47].

Two possible scenarios could be reviewed. The first scenario comprises directing filtered seawater to an MD plant composed of serial and parallel MD staging. The brine is fed either to a thermal crystallizer and/or to a solar pond. The second scenario involves the processing of RO, electrodialysis, multistage flash desalination brines to multi-stage MD with and without circulation; the

final fractional crystallization is achieved via solar/thermal pond system.

In this section, preliminary estimation of the amounts of raw salts that could be produced from these scenarios was investigated. A block flow diagram for the proposed scenarios, based on 40,000 m^3/d feed to VMD and solar pond, is presented in Figure 9. The amounts of salts were determined by overall mass balance calculations. The mass balance calculations were based on performance indicators and main technical specifications for the proposed processes as depicted from the results of this study for PVL HF membrane and other published work [48–50]. Some technical aspects regarding the suggested scenarios and expected salts produced are shown in Table 5.

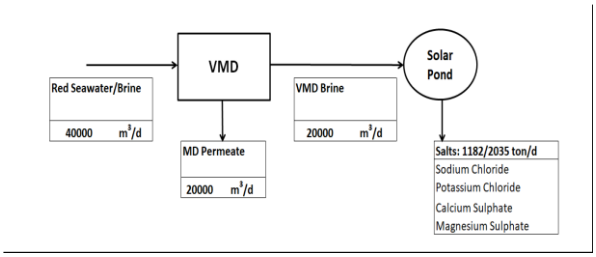

Fig.9. Block flow diagram **for the VMD/solar pond proposed scenarios**

Table 4.: Comparison of the main characteristics and VMD performance data for PVDF HF membranes

Solvent/ additives	Contact angle, ^{o}	Porosity, %	Operating conditions	VMD flux, L/m^2h	Ref.
Pure water					
DMAc/H_2O/LiCl	78-82		10 L/h, 50^{o}C	0.5	[37]
DMF/PVP	82-91	74-83	32 L/h, 50^{o}C	12.5	[30]
NMP/DMF/PVP/Maleic anhydride	-	70-83.4	6 L/h, 50^{o}C	15-41	[21]
NMP/H_2O/PVP	-	77-92	27 L/h, 50^{o}C	9.5	[31]
DMAc/PG	-	-	27 L/h, 50-70^{o}C	40	[36]
NMP/LiCl	130	-	30 L/h, 80^{o}C	1.9	[4]
(DMF,DMAc)/PEG	114	78	12 L/h, 70^{o}C	37.2	This work
(DMF,DMAc)/PEG/LiCl	115	83.4	12L/h, 70^{o}C	48	
Saline solutions					
Tianjin Polytechnic	-	85	3.5% NaCl, 70^{o}C	28	[38]
			SW, 70^{o}C	20	
NMP/LiCl	130	-	8% NaCl, 30 L/h, 80^{o}C	1.13	[4]
DMAc/LiCl/PEG	100.8	69-79	9% NaCl, 65^{o}C	23	[28]
DMF/PVP	82-91	74-83	SSW, 32 L/h, 50^{o}C	12	[30]
NMP/H_2O/PVP	-	77-92	SSW, 27 L/h, 50^{o}C	14.5	[31]
(DMF,DMAc)/PEG	-	-	Red SW	8	[39]
(DMF,DMAc)/PEG	114	78	Med. SW, 12 L/h, 70^{o}C,	23	This work
		78	Red SW, 12 L/h, 70^{o}C	18	
		78	Brine, 12 L/h, 70^{o}C	14	
(DMF,DMAc)/PEG/LiCl	**115**	83.4	Med. SW, 12 L/h, 70^{o}C	32	
		83.4	Red SW, 12 L/h, 70^{o}C	25	
		83.4	Brine, 12 L/h, 70^{o}C	19	

Table 5: Technical aspects of the proposed 40,000 m^3/d VMD/solar pond scenarios and expected salts produced

Feed	VMD	Pond	Expected salts, ton/d
Red Sea water TDS: 44,200 mg/L	VMD flux: 25 L/m^2h Recovery: 50% Membrane area: 33333 m^2	Concentration factor: 0.89	NaCl (895), KCl (27), $CaSO_4$ (43), $MgSO_4$ (216)
Red Sea water RO brine TDS: 73,870 mg/L[51]	VMD flux: 19 L/m^2h Recovery: 50% Membrane area: 43860 m^2	Precipitation efficiency: 65%	NaCl (1587), (40),$CaSO_4$ (70), $MgSO_4$ (338)

4. Conclusion

VMD of Mediterranean Sea water, Red Sea water and Red Sea brine was investigated using two fabricated hydrophobic PVDF HF membranes with and without lithium chloride (PV and PVL, respectively). Addition of lithium chloride enhanced the membrane porosity, mean pore size, surface roughness and introduced more sponge like structure. The VMD system was operated with an energy conservation mode due to complete or partial recirculation, simulating multistage processing at 70ºC. Processing of the different saline streams under VMD mode enabled promising flux approaching 14-23 L/m^2h for PV and 19-32 L/m^2h for PVL HF membranes. Two empirical correlations have been formulated representing the relation between flux and the studied feed salinities for the two prepared membranes. In addition, two VMD/solar pond scenarios were proposed for processing of seawater and RO brine and investigated for water production and salt recovery. The results obtained enable brine concentration to almost salt saturation conditions enabling recovery of valuable salts.

5. Conflicts of interest

"There are no conflicts to declare".

6. Acknowledgments

This work was supported by the Science and Technology Development Fund (STDF) of Egypt [grant number STDF/3991].

7. References

[1] E. Drioli, A. Ali, F. Macedonio, Membrane distillation: Recent developments and perspectives, Desalination. 356 (2015) 56–84. https://doi.org/10.1016/j.desal.2014.10.028.

[2] M.K. Alsebaeai, A.L. Ahmad, Membrane distillation: Progress in the improvement of dedicated membranes for enhanced hydrophobicity and desalination performance, J. Ind. Eng. Chem. 86 (2020) 13–34. https://doi.org/10.1016/j.jiec.2020.03.006.

[3] P. Das, S. Dutta, K.K. Singh, Insights into membrane crystallization: A sustainable tool for value added product recovery from effluent streams, Sep. Purif. Technol. 257 (2021) 117666. https://doi.org/10.1016/j.seppur.2020.117666.

[4] A.C. Sun, W. Kosar, Y. Zhang, X. Feng, Vacuum membrane distillation for desalination of water using hollow fiber membranes, J. Memb. Sci. 455 (2014) 131–142. https://doi.org/10.1016/j.memsci.2013.12.055.

[5] N. Peng, N. Widjojo, P. Sukitpaneenit, M.M. Teoh, G.G. Lipscomb, T.S. Chung, J.Y. Lai, Evolution of polymeric hollow fibers as sustainable technologies: Past, present, and future, Prog. Polym. Sci. 37 (2012) 1401–1424. https://doi.org/10.1016/j.progpolymsci.2012.01.001.

[6] A. Figoli, S. Simone, A. Criscuoli, S.A. Al-Jlil, F.S. Al Shabouna, H.S. Al-Romaih, E. Di Nicolò, O.A. Al-Harbi, E. Drioli, Hollow fibers for seawater desalination from blends of PVDF with different molecular weights: Morphology, properties and VMD performance, Polymer (Guildf). 55 (2014) 1296–1306. https://doi.org/10.1016/j.polymer.2014.01.035.

[7] A. Dastbaz, J. Karimi-Sabet, H. Ahadi, Y. Amini, Preparation and characterization of novel modified PVDF-HFP/GO/ODS composite hollow fiber membrane for Caspian Sea water desalination, Desalination. 424 (2017) 62–73. https://doi.org/10.1016/j.desal.2017.09.030.

[8] H. Kim, T. Yun, S. Hong, S. Lee, Experimental and theoretical investigation of a high performance PTFE membrane for vacuum-membrane distillation, J. Memb. Sci. 617 (2021) 118524. https://doi.org/10.1016/j.memsci.2020.118524.

[9] P. Wang, T.S. Chung, Recent advances in membrane distillation processes: Membrane development, configuration design and application exploring, J. Memb. Sci. 474 (2015) 39–56. https://doi.org/10.1016/j.memsci.2014.09.016.

[10] Q. Ma, A. Ahmadi, C. Cabassud, Direct integration of a vacuum membrane distillation module within a solar collector for small-scale units adapted to seawater desalination in remote places: Design, modeling & evaluation of a flat-plate equipment, J. Memb. Sci. 564 (2018) 617–633. https://doi.org/10.1016/j.memsci.2018.07.067.

[11] Q. Li, L.J. Beier, J. Tan, C. Brown, B. Lian, W. Zhong, Y. Wang, C. Ji, P. Dai, T. Li, P. Le Clech, H. Tyagi, X. Liu, G. Leslie, R.A. Taylor, An integrated, solar-driven membrane distillation system for water purification and energy generation, Appl. Energy. 237 (2019) 534–548. https://doi.org/10.1016/j.apenergy.2018.12.069.

[12] E. Drioli, A. Criscuoli, E. Curcio, Integrated

membrane operations for seawater desalination, Desalination. 147 (2002) 77–81. https://doi.org/10.1016/S0011-9164(02)00579-9.
[13] B. Van Der Bruggen, Integrated membrane separation processes for recycling of valuable wastewater streams: Nanofiltration, membrane distillation, and membrane crystallizers revisited, Ind. Eng. Chem. Res. 52 (2013) 10335–10341. https://doi.org/10.1021/ie302880a.
[14] P. Wang, T.S. Chung, A new-generation asymmetric multi-bore hollow fiber membrane for sustainable water production via vacuum membrane distillation, Environ. Sci. Technol. 47 (2013) 6272–6278. https://doi.org/10.1021/es400356z.
[15] C.A. Quist-Jensen, F. Macedonio, E. Drioli, Membrane crystallization for salts recovery from brine—an experimental and theoretical analysis, Desalin. Water Treat. 57 (2016) 7593–7603. https://doi.org/10.1080/19443994.2015.1030110.
[16] C.A. Quist-Jensen, A. Ali, E. Drioli, F. Macedonio, Perspectives on mining from sea and other alternative strategies for minerals and water recovery – The development of novel membrane operations, J. Taiwan Inst. Chem. Eng. 94 (2019) 129–134. https://doi.org/10.1016/j.jtice.2018.02.002.
[17] Z. Yan, H. Yang, H. Yu, F. Qu, H. Liang, B. Van Der Bruggen, G. Li, Reverse osmosis brine treatment using direct contact membrane distillation (DCMD): Effect of membrane characteristics on desalination performance and the wetting phenomenon, Environ. Sci. Water Res. Technol. 4 (2018) 428–437. https://doi.org/10.1039/c7ew00468k.
[18] Y. Xu, Y. Yang, M. Sun, X. Fan, C. Song, P. Tao, M. Shao, High-performance desalination of high-salinity reverse osmosis brine by direct contact membrane distillation using superhydrophobic membranes, J. Appl. Polym. Sci. 138 (2021) 1–10. https://doi.org/10.1002/app.49768.
[19] S.R. Tewfik, M.H. Sorour, A.M.G. Abulnour, H.F. Shaalan, H.A. Hani, M.M.H. El-Sayed, Y.O. Abdelrahman, E.S. Sayed, A.N. Mohamed, A.A. Al-Mansoup, N.A. Shawky, Membrane Materials Design Trends, first, CRC Press 6000 Broken Sound Parkway NW, suite 300, Boca Raton, FL 33487-2742, Taylor & Francis Group, 2020. https://doi.org/10.1201/9780429020254-2.
[20] S.R. Tewfik, M.H. Sorour, H.F. Shaalan, H.A. Hani, Effect of spinning parameters of polyethersulfone based hollow fiber membranes on morphological and mechanical properties, Membr. Water Treat. 9 (2018) 43–51. https://doi.org/10.12989/mwt.2018.9.1.043.
[21] E. Drioli, A. Ali, S. Simone, F. Macedonio, S.A. Al-Jlil, F.S. Al Shabonah, H.S. Al-Romaih, O. Al-Harbi, A. Figoli, A. Criscuoli, Novel PVDF hollow fiber membranes for vacuum and direct contact membrane distillation applications, Sep. Purif. Technol. 115 (2013) 27–38. https://doi.org/10.1016/j.seppur.2013.04.040.
[22] W.R. Bowen, A.W. Mohammad, N. Hilal, Characterisation of nanofiltration membranes for predictive purposes - Use of salts, uncharged solutes and atomic force microscopy, J. Memb. Sci. 126 (1997) 91–105. https://doi.org/10.1016/S0376-7388(96)00276-1.
[23] E. Yuliwati, A.F. Ismail, Effect of additives concentration on the surface properties and performance of PVDF ultrafiltration membranes for refinery produced wastewater treatment, Desalination. 273 (2011) 226–234. https://doi.org/10.1016/j.desal.2010.11.023.
[24] D. Hou, J. Wang, D. Qu, Z. Luan, C. Zhao, X. Ren, Preparation of hydrophobic PVDF hollow fiber membranes for desalination through membrane distillation, Water Sci. Technol. 59 (2009) 1219–1226. https://doi.org/10.2166/wst.2009.080.
[25] E. Fontananova, J.C. Jansen, A. Cristiano, E. Curcio, E. Drioli, Effect of additives in the casting solution on the formation of PVDF membranes, Desalination. 192 (2006) 190–197. https://doi.org/10.1016/j.desal.2005.09.021.
[26] D. Hou, J. Wang, D. Qu, Z. Luan, X. Ren, Fabrication and characterization of hydrophobic PVDF hollow fiber membranes for desalination through direct contact membrane distillation, Sep. Purif. Technol. 69 (2009) 78–86. https://doi.org/10.1016/j.seppur.2009.06.026.
[27] L. Zheng, Z. Wu, Y. Wei, Y. Zhang, Y. Yuan, J. Wang, Preparation of PVDF-CTFE hydrophobic membranes for MD application: Effect of LiCl-based mixed additives, J. Memb. Sci. 506 (2016) 71–85. https://doi.org/10.1016/j.memsci.2016.01.044.
[28] Y. Tang, N. Li, A. Liu, S. Ding, C. Yi, H. Liu, Effect of spinning conditions on the structure and performance of hydrophobic PVDF hollow fiber membranes for membrane distillation, Desalination. 287 (2012) 326–339. https://doi.org/10.1016/j.desal.2011.11.045.
[29] A. Mansourizadeh, A.F. Ismail, Effect of LiCl concentration in the polymer dope on the structure and performance of hydrophobic PVDF hollow fiber membranes for CO2 absorption, Chem. Eng. J. 165 (2010) 980–988. https://doi.org/10.1016/j.cej.2010.10.034.
[30] S. Simone, A. Figoli, A. Criscuoli, M.C. Carnevale, A. Rosselli, E. Drioli, Preparation of hollow fibre membranes from PVDF/PVP blends and their application in VMD, J. Memb. Sci. 364 (2010) 219–232. https://doi.org/10.1016/j.memsci.2010.08.013.
[31] S. Simone, A. Figoli, A. Criscuoli, M.C. Carnevale, S.M. Alfadul, H.S. Al-Romaih, F.S. Al Shabouna, O.A. Al-Harbi, E. Drioli, Effect of selected spinning parameters on PVDF hollow fiber morphology for potential application in desalination by VMD, Desalination. 344 (2014) 28–35. https://doi.org/10.1016/j.desal.2014.03.004.
[32] A. Malijevský, A.O. Parry, Modified Kelvin Equations for Capillary Condensation in Narrow and Wide Grooves, Phys. Rev. Lett. 120 (2018) 135701. https://doi.org/10.1103/PhysRevLett.120.135701.

[33] M. Tomaszewska, Preparation and properties of flat-sheet membranes from poly(vinylidene fluoride) for membrane distillation, Desalination. 104 (1996) 1–11. https://doi.org/10.1016/0011-9164(96)00020-3.
[34] D. Wang, K. Li, W.K. Teo, Porous PVDF asymmetric hollow fiber membranes prepared with the use of small molecular additives, J. Memb. Sci. 178 (2000) 13–23. https://doi.org/10.1016/S0376-7388(00)00460-9.
[35] A. Mansourizadeh, A.F. Ismail, A developed asymmetric PVDF hollow fiber membrane structure for CO2 absorption, Int. J. Greenh. Gas Control. 5 (2011) 374–380. https://doi.org/10.1016/j.ijggc.2010.09.007.
[36] L. Zhao, C. Wu, Z. Liu, Q. Zhang, X. Lu, Highly porous PVDF hollow fiber membranes for VMD application by applying a simultaneous co-extrusion spinning process, J. Memb. Sci. 505 (2016) 82–91. https://doi.org/10.1016/j.memsci.2016.01.014.
[37] B. Wu, K. Li, W.K. Teo, Preparation and Characterization of Poly(vinylidene fluoride) Hollow Fiber Membranes for Vacuum Membrane Distillation, J. Appl. Polym. Sci. 106 (2007) 1482–1495.
[38] C. Huayan, W. Chunrui, J. Yue, W. Xuan, L. Xiaolong, Comparison of three membrane distillation confi gurations and seawater desalination by vacuum membrane distillation, Desalin. Water Treat. 28 (2011) 321–327. https://doi.org/10.5004/dwt.2011.1605.
[39] H.J. Joo, H.Y. Kwak, Experimental evaluation for the freshwater production characteristics according to the salinity conditions of vacuum membrane distillation module, Desalin. Water Treat. 57 (2016) 10005–10011. https://doi.org/10.1080/19443994.2015.1040267.
[40] Y. Wang, Z. Xu, N. Lior, H. Zeng, An experimental study of solar thermal vacuum membrane distillation desalination, Desalin. Water Treat. 53 (2015) 887–897. https://doi.org/10.1080/19443994.2014.927187.
[41] X. Wang, L. Zhang, H. Yang, H. Chen, Feasibility research of potable water production via solar-heated hollow fiber membrane distillation system, Desalination. 247 (2009) 403–411. https://doi.org/10.1016/j.desal.2008.10.008.
[42] Y.D. Kim, K. Thu, S.H. Choi, Solar-assisted multi-stage vacuum membrane distillation system with heat recovery unit, Desalination. 367 (2015) 161–171. https://doi.org/10.1016/j.desal.2015.04.003.
[43] H.W. Chung, J. Swaminathan, D.M. Warsinger, J.H. Lienhard V, Multistage vacuum membrane distillation (MSVMD) systems for high salinity applications, J. Memb. Sci. 497 (2016) 128–141. https://doi.org/10.1016/j.memsci.2015.09.009.
[44] B.L. Pangarkar, S.K. Deshmukh, P. V. Thorat, Energy efficiency analysis of multi-effect membrane distillation (MEMD) water treatment, Int. J. ChemTech Res. 9 (2016) 279–289.
[45] E.S. Mohamed, P. Boutikos, E. Mathioulakis, V. Belessiotis, Experimental evaluation of the performance and energy efficiency of a Vacuum Multi-Effect Membrane Distillation system, Desalination. 408 (2017) 70–80. https://doi.org/10.1016/j.desal.2016.12.020.
[46] A. Omar, A. Nashed, Q. Li, R.A. Taylor, Experimental and numerical evaluation of the energy requirement of multi-stage vacuum membrane distillation designs, Sep. Purif. Technol. 257 (2021) 117303. https://doi.org/10.1016/j.seppur.2020.117303.
[47] Y. lei Xing, C. hua Qi, H. jun Feng, Q. chun Lv, G. rong Xu, H. qing Lv, X. Wang, Performance study of a pilot-scale multi-effect vacuum membrane distillation desalination plant, Desalination. 403 (2017) 199–207. https://doi.org/10.1016/j.desal.2016.07.008.
[48] I.C. Watson, O.J. Morin, L. Henthorne, Desalting Handbook for Planners, Desalin. Water Purif. Res. Dev. Progr. Rep. (2003) 1–310. http://www.ncbi.nlm.nih.gov/pubmed/22126638.
[49] F.A. Rodríguez, D.E. Santiago, N.F. Suárez, J.A. Ortega Méndez, J.M. Veza, Comparison of evaporation rates for seawater and brine from reverse osmosis in traditional salt works: Empirical correlations, Water Sci. Technol. Water Supply. 12 (2012) 234–240. https://doi.org/10.2166/ws.2012.133.
[50] H.Z. Harraz, Topic 11 : EVAPORITE SALT DEPOSITS Outline of Topic 11 :, (2016). https://doi.org/10.13140/RG.2.1.3231.3203.
[51] M.H. Sorour, H.A. Hani, H.F. Shaalan, G.A. Al-Bazedi, Schemes for salt recovery from seawater and RO brines using chemical precipitation, Desalin. Water Treat. 55 (2015) 2398–2407. https://doi.org/10.1080/19443994.2014.946720.